CRREL

REPORT 79-23

Effects of seasonal changes and ground ice on electromagnetic surveys of permafrost

Effects of seasonal changes and ground ice on electromagnetic surveys of permafrost

Steven A. Arcone, Allan J. Delaney and Paul V. Sellmann

October 1979

Cover: Massive ice exposed in a road cut near Fox, Alaska. The length of the boom is 3.66 m.

REPORT DOCUMENTATION PAGE		READ INSTRUCTIONS BEFORE COMPLETING FORM
1. REPORT NUMBER CRREL Report 79-23	2. GOVT ACCESSION NO.	3. RECIPIENT'S CATALOG NUMBER
4. TITLE (and Subtitle) EFFECTS OF SEASONAL CHANGES AND GROUND ICE ON ELECTROMAGNETIC SURVEYS OF PERMAFROST		5. TYPE OF REPORT & PERIOD COVERED
		6. PERFORMING ORG. REPORT NUMBER
7. AUTHOR(s) Steven A. Arcone, Allan J. Delaney and Paul V. Sellmann		8. CONTRACT OR GRANT NUMBER(s)
9. PERFORMING ORGANIZATION NAME AND ADDRESS U.S. Army Cold Regions Research and Engineering Laboratory Hanover, NH 03755		10. PROGRAM ELEMENT, PROJECT, TASK AREA & WORK UNIT NUMBERS DA Project 4A762730AT42 Task D; Work Unit 013
11. CONTROLLING OFFICE NAME AND ADDRESS Directorate of Military Programs		12. REPORT DATE October 1979
Office, Chief of Engineers Washington, D.C. 20314		13. NUMBER OF PAGES 29
14. MONITORING AGENCY NAME & ADDRESS(If different from Controlling Office)		15. SECURITY CLASS. (of this report) Unclassified
		15a. DECLASSIFICATION/DOWNGRADING SCHEDULE

16. DISTRIBUTION STATEMENT (of this Report)

Approved for public release; distribution unlimited.

17. DISTRIBUTION STATEMENT (of the abstract entered in Block 20, if different from Report)

18. SUPPLEMENTARY NOTES

19. KEY WORDS (Continue on reverse side if necessary and identify by block number)

Electromagnetic ground resistivity technique   Seasonal variations
Fairbanks, Alaska
Ground ice
Permafrost
Prudhoe Bay

20. ABSTRACT (Continue on reverse side if necessary and identify by block number)
The performance of surface impedance and magnetic induction electromagnetic subsurface exploration techniques was studied seasonally at various sites in Alaska where permafrost and massive ground ice occurred. The surface impedance method, which uses radiowaves in the LF and VLF bands, and the magnetic induction method, which uses low-frequency magnetic induction fields, distinguish subsurface materials by the electrical resistivity of the materials. The methods used have greatest sensitivity within about 20 m of the surface and are, therefore, most applicable for shallow subsurface investigations. The selection of study sites was based on anticipated contrasts in electrical resistivity between ground ice and adjacent earth materials. A magnetic induction instrument, using a separation of 3.66-m between the transmitter and receiver antennas, in general was able to detect near-surface zones of massive ice and to

DD FORM 1473   1 JAN 73   EDITION OF 1 NOV 65 IS OBSOLETE

20. Abstract (cont'd)

provide data regarding permafrost distribution in both the Fairbanks and Prudhoe Bay areas. At this antenna separation, the depth of magnetic field penetration was sufficient to include mainly the zone containing maximum contrasts in resistivity between ground ice and other earth materials. In the Fairbanks area, contrasts in this zone were greatest in late winter when the seasonally thawed surface layer was completely frozen. When thawed, this layer usually becomes more conductive and often masks the deeper resistivity contrasts. In the Prudhoe Bay area, maximum ground resistivity contrasts were detected in late summer when shallow subsurface temperatures had risen sufficiently to permit resistivity contrasts between the massive ice and the ice-rich ground to appear. Use of the surface impedance method between 200 and 400 kHz revealed resistivity anomalies that qualitatively agreed with massive ice zones in both the Fairbanks and Prudhoe Bay areas. However, in some cases the results were misleading, most likely because of the plane wave assumptions used for data interpretation. On the basis of the studies presented, it is concluded that the magnetic induction method was generally superior to the surface impedance method for delineating permafrost and zones of massive ground ice because the magnetic induction fields were local and well defined and because antenna loop spacing and orientation could be varied to help discriminate subsurface features. Also, it is concluded that the optimum time of year to perform electromagnetic surveys at shallow depths is not necessarily when the electromagnetically absorbing surface layer is frozen. At this time of year, ground temperatures may be so low in some geographic regions that resistivity contrasts between frozen earth and massive ice are eliminated. Therefore, in planning a survey, careful attention must be paid to the geological and thermal aspects of a site or region.

PREFACE

CONTENTS

ILLUSTRATIONS

EFFECTS OF SEASONAL CHANGES AND GROUND ICE ON ELECTROMAGNETIC SURVEYS OF PERMAFROST

Steven A. Arcone, Allan J. Delaney and Paul V. Sellmann

INTRODUCTION

Background

Electromagnetic geophysical methods that operate at frequencies below 1 MHz are based on natural contrasts in the electrical properties of different earth materials. Many of these methods utilize energy and coupling mechanisms that usually effectively penetrate only about 20 m below the ground surface. In permafrost regions, this depth commonly covers the variable surface zone in which the greatest fluctuations in seasonal temperature occur and in which most massive ice is found. The large seasonal changes in ice volume, soil moisture and temperature found in this zone, which mainly determine the electrical properties of resistivity and permittivity, have an important bearing on the results of a prospective electromagnetic survey designed for shallow ground exploration.

Previous field investigations of the effect of seasonal changes in the electrical properties of the earth upon the performance of electromagnetic techniques have used several methods. MacKay (1969) investigated several Pleistocene geologic features in the Mackenzie Delta region using direct-current multiprobe arrays. Although his measurements were not made seasonally, he documented resistivity contrasts found between frozen and thawed states of several material types. Wong et al. (1977) and Rossiter et al. (1978) reported on seasonal variations in the Tuktoyaktuk area of the Canadian NWT using audiofrequency/magnetotelluric (AMT), radio interferometry and in-situ antenna impedance techniques at a variety of frequencies. The measurements of Wong et al. and Rossiter et al. were carried out over large ground ice features overlain by several meters of clay till. They stated that differences between their summer and winter AMT soundings were not significant because the extremely low frequencies

used are insensitive to active layer changes. However, the reports of seasonal contrasts in the electrical properties of the clay till obtained by them, using very high frequency in-situ antenna impedance techniques, were extremely large and were due to the very high water content of the till.

Hoekstra et al. (1975), Hoekstra (1978), and Rennie et al. (1978) reported on investigations in Fairbanks, Alaska, the Mackenzie Valley and northern Alberta, using the radiowave and magnetic induction techniques described in the present report. Their investigations were performed primarily for mapping the lateral and vertical distributions of permafrost and did not include seasonal observations. A seasonal study utilizing the techniques covered in this report was made by Delaney et al. (1978).

Recently, attempts have been made to detect massive ground ice features by electromagnetic pulse techniques. Observations using radar have been reported by Kovacs and Morey (1979), Annan and Davis (1976), and Davis et al. (1976).

Objectives and procedures

The objectives of this study were to determine the influence of seasonal changes in permafrost areas, and ground ice content and distribution, upon radiowave surface impedance in the VLF and LF bands and upon magnetic induction coupling at close antenna spacings of 30 m and less. Several sites within Alaska's continuous and discontinuous permafrost zones were chosen for study. At each of these sites, the actual geology was obtained from past drilling or was inferred from surface features. Most of these sites were characterized by lateral inhomogeneities (ice masses), a significant departure from the vertical layering ideal that can more readily be analyzed mathematically. Data were acquired in each surveyed area along either single
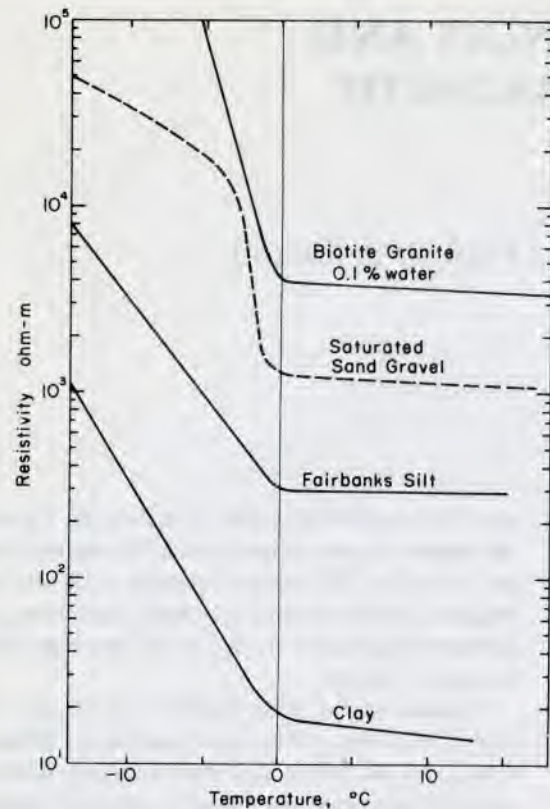
Figure 1. Resistivities of three sediment types and one rock type as a function of temperature (after Hoekstra and McNeill 1973).

profiles or over a grid network. Most observations were made both in late winter and in late summer to evaluate seasonal effects. At some sites where massive ice studies were conducted near Prudhoe Bay, data were not taken seasonally at the same locations, although ground conditions at the various sites were similar.

GROUND ELECTRICAL RESISTIVITY IN PERMAFROST REGIONS

Surface determinations of ground resistivity in permafrost regions are influenced by the resistivities of the individual materials present and by their stratifications. For each permafrost material, mineralogy, porosity, permeability, free water content, and ionic concentration within the free water are important resistivity factors just as they are for nonpermafrost materials. However, in permafrost regions, additional factors such as ice content (extremely high resistivities are normally exhibited by ground ice), seasonal changes in temperature, and distribution of frozen or thawed material also influence resistivity. Changes in material properties due

to annual variations in temperature can cause ground resistivity in some places to change by two to three orders of magnitude in the course of a year.

Figure 1 (after Hoekstra and McNeill 1973) illustrates the effect of temperature upon resistivity for three sediment types and one rock type. As temperature decreases below 0°C, resistivity increases because of the continuing increase of the proportion of frozen to unfrozen water through various large and small-scale effects. At grain-size dimensions, unfrozen water often remains adsorbed on soil particle or rock grain surfaces, but continually freezes as temperature decreases. On larger scales, ice lenses and massive features such as ice wedges commonly form in silts and clays. In addition, pingo ice can be found in some environments. Pingos, wedges and lenses may occur in some places with horizontal or vertical dimensions of many meters. Discussions of massive ice formation are presented by Lachenbruch (1962), Hopkins et al. (1955) and Péwé (1974).

A surface measurement of resistivity in geophysical prospecting is also influenced by the natural resistivity stratification or layering of earth materials. Stratification in permafrost is common even in uniform materials, primarily because of changes in temperature with depth. An example of the annual variations in ground temperature is given in Figure 2; the temperatures were recorded near Fairbanks in the discontinuous permafrost zone by Crory (1960). These observations were made at the CRREL permafrost test site in Fairbanks where the subsurface consists of perennially frozen organic silt containing varying amounts of ground ice. The data were then replaced by laboratory determinations of resistivity versus temperature (Fig. 3 after Hoekstra et al. 1975) for saturated organic silt, to give a hypothetical illustration of the influence of these seasonal temperature changes on ground resistivity (Fig. 4). Figure 4 indicates the significant annual variations in resistivity that can occur in the upper 5 meters at this site.

In some cases, reversals of the resistivity gradient with depth can exist, even in a single material type. This may occur when the seasonal active layer does not freeze down to the permafrost, thus presenting three or four reversals (e.g., from seasonal frost to seasonal thaw, to permafrost, and to perennial thaw). This can be additionally complicated by horizontal variations in the gradient. Additional complications occur when perennial thaw zones (taliks) exist within permafrost.

The above thermally controlled resistivity variations must then be superimposed on all other natural variations with depth related to material properties. Therefore, in some geological settings, the factors affecting
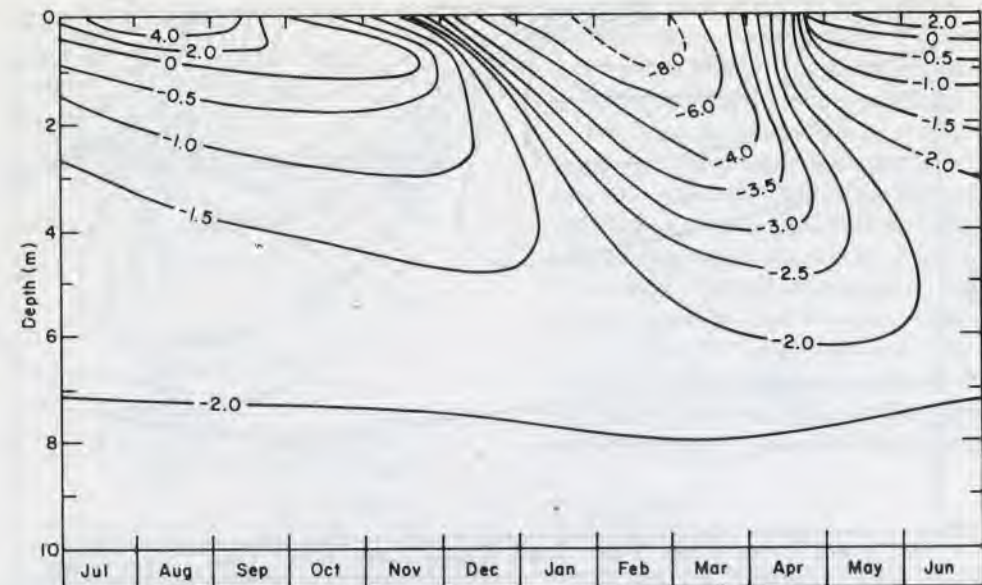
Figure 2. Temperatures (°C) as a function of depth and time of year for ice-rich organic silt at the Farmers Loop Test Site in Fairbanks, Alaska (after Crory 1960).
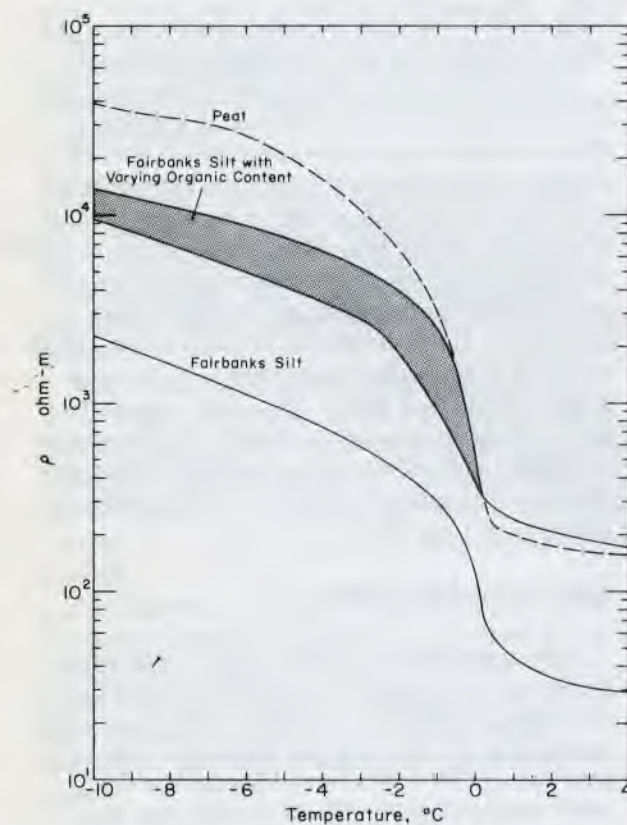
Figure 3. Resistivities of several soils commonly found near Fairbanks, Alaska, as a function of temperature (after Hoekstra et al. 1975).

the application of geophysical methods for permafrost distribution and ground ice investigations can be extremely complex. Ideally then, performance studies of geophysical equipment in permafrost should include studies where the ground is fairly homogeneous, both mineralogically and by grain size. This would help to eliminate some of the variables that influence the results.

ELECTROMAGNETIC TECHNIQUES

General

Electromagnetic methods that distinguish geological changes by the changes in electrical properties may be divided into two categories: pulse and steady-state methods. Pulse methods perform the same function as seismic or sonar profiling and are referred to as radio-echo sounding and subsurface radar profiling (Annan and Davis 1976). The frequencies used are usually between 35 and 150 MHz, where atomic and molecular polarization properties, especially those of water, are as important as resistivity. As with lower frequencies, subsurface penetration at these frequencies is limited by the ground conductivity (the inverse of resistivity). Therefore, these methods find their best application in highly resistive (i.e., poorly conducting or lossless) dielectrics such as ice, cold ice-rich soil, or gravel-rich sandy soils (i.e. usually materials containing small quantities of free water).

2

3
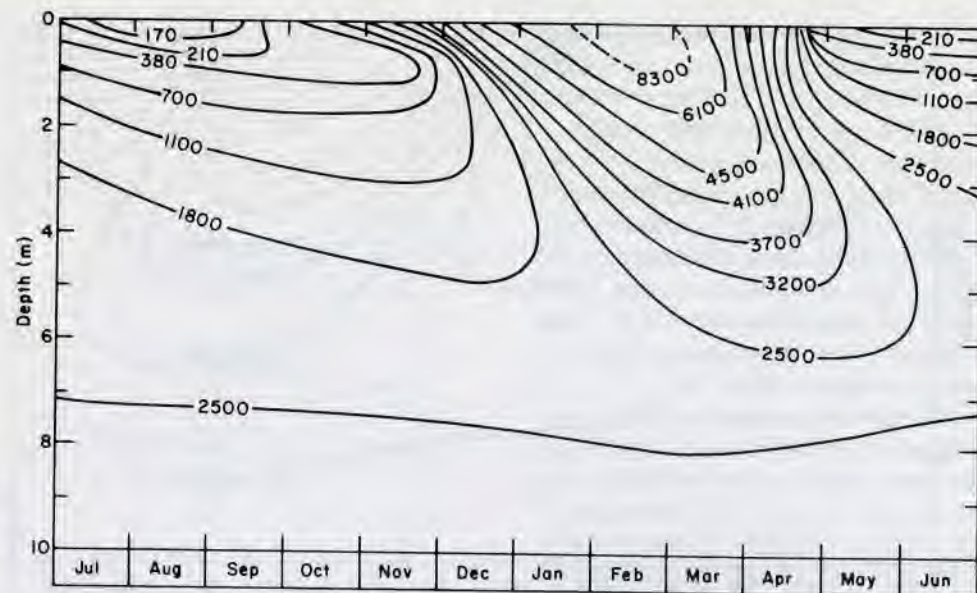
Figure 4. Annual temperature data from Figure 2 translated into equivalent resistivity values based on laboratory measurements for organic silt of Hoekstra et al. (1975) shown in Figure 3.

The steady-state category includes direct current (DC), magnetic induction (MI), and surface impedance (SI) methods. In all these methods, for interpretation purposes, the steady-state configurations of electrical or magnetic fields varying at frequencies below about 1MHz* are compared with theoretical data generated from models of layered gound or from models of in-homogeneities. All these methods are sensitive primarily to the values and variations of resistivity.

Subsurface observations at increasing depths are made by increasing the spacing of excitation electrodes to deepen the current penetration (DC technique), by increasing the spacing of loop antennas to deepen the magnetic field penetration (MI technique), or by selecting lower transmitting frequencies to obtain an increased radiowave penetration (SI technique). In the latter case, when frequencies below about 10 kHz are used, the technique is referred to as magnetotelluric or audio-frequency/magnetotelluric (Cagniard 1953, Telford et al. 1976) because of the natural sources used for wave generation. Above 10 kHz, the energy sources are artificial. At all frequencies, however, the SI technique compares the orthogonal earth tangential components of electric and magnetic fields with each other. This

comparison is known as the surface impedance, so we refer to its use as the surface impedance technique.

As mentioned earlier, the studies in this report primarily discuss the use of the MI and SI techniques. Recent commercial advances in equipment portability and ease of operation have made these techniques very promising for rapid exploration of the upper 10-20 m of the earth. In addition, theoretical SI studies by Hughes and Wait (1975) have shown that the simple, layered model interpretation of data can be applied to local layering, the lateral dimensions of which are very much smaller than a free-space wavelength (e.g., the wave-length at 300 kHz is 1 km). This point in particular is demonstrated by some of our results. The frequencies employed for the SI method are between 10 kHz and 400 kHz. The antenna spacings for the MI technique are between 3 and 30 m.

Magnetic induction method

This method derives ground resistivity values from the amount of magnetic field coupling between two loop antennas located at, or slightly above, the earth's surface (Fig. 5). One loop, the transmitter antenna, generates a primary time harmonic magnetic field, which couples directly with the receiver loop, but also induces electrical currents (sometimes referred to as "eddy" currents) within the ground. These currents then generate a secondary magnetic field, which also couples with the receiver loop. The primary and secondary
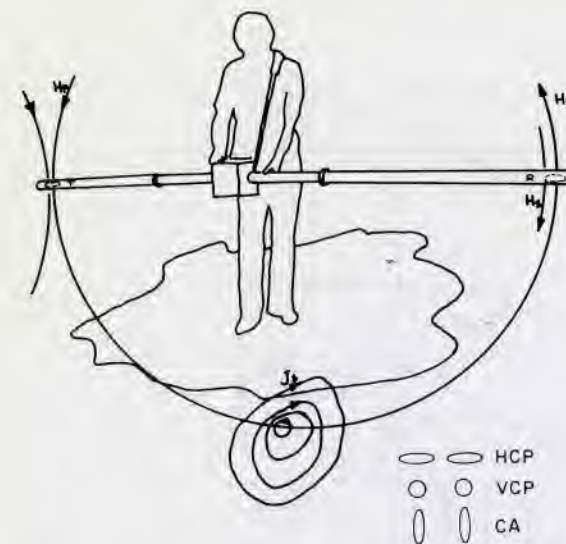
Figure 5. Magnetic induction instrument (Geonics EM31) for measuring ground resistivity. The transmitting loop T produces a primary magnetic field H_p which induces eddy currents J_e within the ground. J_e then produces a secondary magnetic field H_s which is received out of phase with H_p at the receiver R. The quadrature phase component of H_s/H_p is calibrated in mhos/m of conductivity. Also shown are some of the possible loop orientations, two of which, HCP and VCP, are possible with the Geonics EM31.

coupling depend on loop orientation and separation, but the secondary coupling depends on ground conductivity as well. The ratio of secondary to primary coupling is usually simply calibrated against conductivity (discussed below) so that this ratio is the quantity measured.

Information about resistivity variations with depth are achieved by varying either the interloop spacing or the loop orientation. Some of the different loop orientations are also shown in Figure 5. They are defined as vertical coplanar (VCP), horizontal coplanar (HCP) and coaxial (CA). Other, asymmetric configurations are also possible.

The magnetic coupling is determined usually from the mutual impedance Z defined as V/I, where V is the voltage in the transmitter loop and I is the current induced in the receiver loop. Z is usually normalized by the free space impedance Z_0 (in effect, a measure of the primary coupling), which is determined by the formula

$$Z_0 = \frac{i\mu_0\omega(n_tA_t)(n_rA_r)}{4\pi r^3} \quad (1)$$

where ω is the frequency in radians per second, $\mu_0 =$

$4\pi \times 10^{-7}$ Henry/m, $i = \sqrt{-1}$, nA is the product of turns n and area A of the transmit (t) and receive (r) loop antennas, and r is the loop separation.

For these studies, the Geonics* EM31 and EM34 instruments were used. Both instruments may be employed in either the HCP or the VCP mode and the EM34 can also be used in the CA mode. The EM31 uses antenna loops spaced 3.66 m apart and operates at 39 kHz.[†] The EM34 operates at 1.6 kHz and can be used at either 15 or 30-m loop separations.

Both the EM31 and EM34 instruments have been designed so that, after the primary coupling has been eliminated, the ratio Z/Z_0 may be well approximated for homogeneous ground by the formula

$$\frac{Z}{Z_0} = \left(\frac{\gamma r}{2}\right)^2. \quad (2)$$

The quantity γ is related to the conductivity σ (the inverse of resistivity ρ) by the formula

$$\gamma = \sqrt{i\omega\mu_0\sigma} \quad (3)$$

so that eq 2 becomes

$$\frac{Z}{Z_0} = \frac{i\mu_0\omega\sigma r^2}{4}. \quad (4)$$

This expression is purely imaginary and shows that the imaginary part (or quadrature phase component) of the normalized mutual impedance has a linear dependence upon conductivity. Equation 4 holds for both HCP and VCP orientations and is an approximation, appropriate for the EM31 and EM34, of the general coupling formulas for homogeneous ground given by Keller and Frischknecht (1966, p. 335). The approximation is valid when the quantity γr is much less than one.

When the earth is layered, an apparent conductivity must then be defined that corresponds to the equivalent conductivity that would produce the same modulus for the mutual impedance above a homogeneous earth. Interpolation curves or computational integrations of integral equations (Keller and Frischknecht 1966, Sinha 1976) must then be used to resolve the different layer resistivities and thicknesses. Appendix A gives a discussion of the depth of sensitivity of the various loop orientations and interloop spacings using two- and three-layer apparent resistivity curves.

The magnetic induction method is most accurate for high conductivities (i.e., > 0.001 mhos/m) and
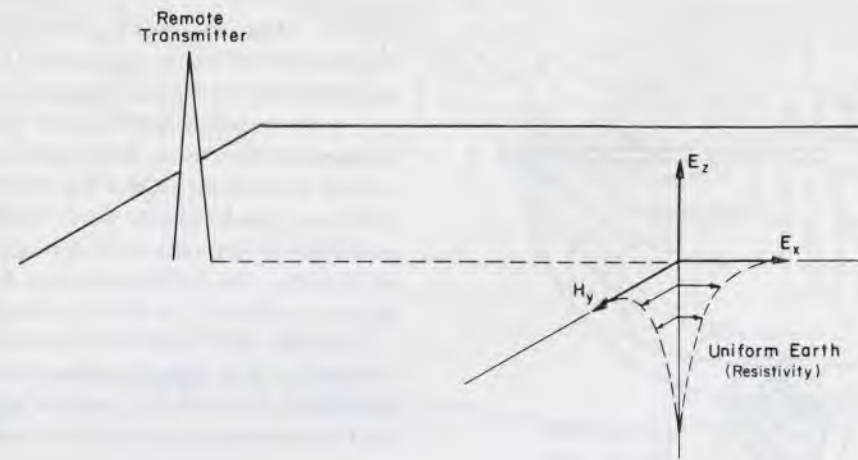
Figure 6. Electromagnetic field components of a vertically polarized radio surface wave. H_y is in the negative y direction.

least accurate for low conductivities; this is because of the difficulty in obtaining a site of extremely high resistivity at which a correct zero point ($\sigma = 0$) calibration can be made. This method then complements the surface impedance method (discussed next), which is more accurate at low conductivities.

Surface impedance (radiowave) method

This method derives ground resistivity values from a comparison between the electromagnetic field components of a propagating ground or sky wave. In the VLF band, powerful transmitters operated by military organizations allow radiation to be monitored over a range of several thousand kilometers. For work in Alaska, the only usable VLF radiation is from station NLK, in Jim Creek, Washington, which radiates 0.5 MW at 18.6 kHz. At this distance, the radiation is in the sky wave mode propagating via one or more skips off the ionosphere. In the LF band, transmitters are available locally in Alaska that radiate between 25 and 1000 W. Consequently, the radiation used for LF surveying is usually in the ground wave mode. The reader is referred to the texts by Stratton (1941) and Jordan and Balmain (1968) for general discussions of these modes. A more advanced discussion is given by Wait (1970).

The electromagnetic field components of a ground or sky wave radiated by a vertically polarized antenna are illustrated in Figure 6. The electric field components E_x and E_z, and the magnetic field component H_y, are referenced to a local, right hand x, y, z coordinate system (H_y is in the negative y direction). The surface impedance Z_s is defined as

$$Z_s \doteq E_x/H_y \Big]_{z=0} \quad {}^* \tag{5}$$

and is a complex quantity having both an amplitude $|Z_s|$ and a phase ϕ as in the expression $Z_s = |Z_s| e^{i\phi}$. At frequencies below about 1 MHz, Z_s is approximated for a uniform subsurface model by the formula

$$Z_s = -\sqrt{\omega\mu_0\rho}\, e^{i45^\circ}. \tag{6}$$

Equation 6 applies when dielectric properties are neglected.

The phase value, 45°, is usually indicative of resistive homogeneity, at least to a depth δ, defined in the literature as the skin depth, and derived from the formula

$$\delta = \sqrt{\frac{2\rho}{\omega\mu_0}}. \tag{7}$$

At this depth, the refracted field strengths have attenuated to e^{-1} of their surface values. Figure 7 shows the variation of δ with frequency for various values of ground resistivity. Because δ depends upon frequency, more than one frequency can be used to resolve resistivity changes with depth. However, in Alaska, adequate field strengths above 10 kHz within the VLF and LF bands are rarely simultaneously available at any one location.

When the earth is layered, eq 6 must be modified because the phase and amplitude of Z_s change, the magnitude of change depending upon the resistivity and

*This definition automatically applies to the ground wave, but for the sky wave the grazing incidence angle must be near 0°, which is usually true at ranges > 1000 km at VLF.
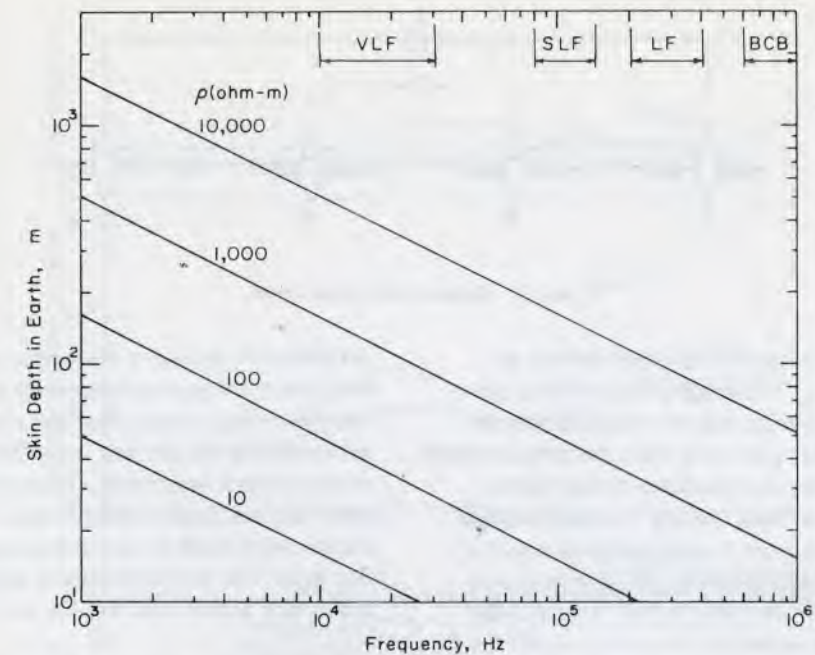

Figure 7. Skin depth of electromagnetic plane waves as a function of frequency and ground resistivity.

thickness of each layer. Wait (1970) presents formulas for generating Z_s values above any number of layers. In general, a phase $> 45^\circ$ usually indicates that resistivity is decreasing with depth, whereas a phase $< 45^\circ$ usually indicates that resistivity is increasing with depth. According to this simplified model of homogeneous layers, all phase angles occur between 0° and 90°. When lateral inhomogeneities exist, the theory does not apply and only qualitative interpretations can be made.

The separate instruments used for measuring resistivity in the VLF and LF bands are similar to each other and commercially available. E_x is determined between two electrode probes inserted in the ground. H_y is measured with a ferrite-loaded coil. The LF device must be pretuned for operation between 200 and 400 kHz, whereas the VLF device operates with pretuned circuits supplied by the manufacturer, each pretuned to one of the few VLF transmitters in use today. The amplitude of Z_s is calibrated in ohm-m of "apparent resistivity" ρ_a (range is 0-30,000 ohm-m), which is determined from the amplitude inversion of eq 6,

$$\rho_a = \frac{|Z_s|^2}{\omega\mu_0}. \tag{8}$$

This value equals the true resistivity when the earth is homogeneous. The phase of Z_s is read directly in degrees (range is 0° to 90°). A high impedance voltmeter is

used to measure E_x so that the contact resistance of the probes does not interfere significantly with the measurement.

The accuracy of the readings depends upon the signal-to-noise ratio. This ratio is mainly determined by transmitter distance and power (for LF and VLF), by ionospheric factors (for VLF), and by the value of ground resistivity itself (for LF and VLF) because as resistivity decreases so does the amplitude of E_x.

Direct current method

This is a standard method for measuring earth resistivity and was used in two of our studies for comparative purposes. A four-terminal, equispaced, colinear, electrode array, termed a *Wenner array* (Wenner 1915), was used, as shown in Figure 8. With the Wenner array, current I is driven through the outer two electrodes P_1 and P_4 and the potential V induced in the earth by this current is measured at the inner pair of electrodes P_2 and P_3. An apparent electrical resistivity of the ground is then computed from the ratio V/I. For a Wenner array, the true resistivity of homogeneous ground is given by the equation

$$\rho = 2\pi a \frac{V}{I} \tag{9}$$

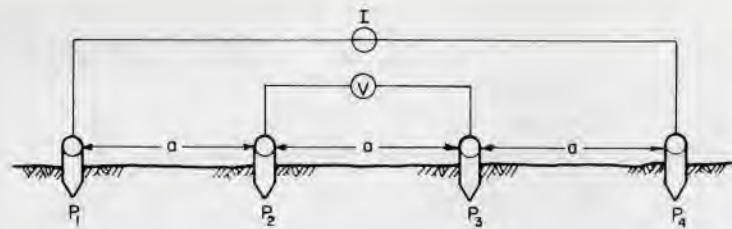where a is the interelectrode spacing.

Figure 8. Wenner electrode array.

When the ground is layered eq 9 then defines an apparent resistivity ρ_a. The spacing a is varied to determine the resistivity layering and the resulting data are then matched to curves generated from theoretical models to resolve the resistivity and thickness of each layer.

In two applications, the a spacing was held constant and all four electrodes were moved simultaneously for profiling purposes. In another case, the a spacing was constantly increased from a fraction of a meter to 20 or 30 m to acquire information on variations with depth. The probes were copper-clad steel and a solution of copper sulfate was poured around each probe to lower contact resistance when frozen ground was encountered. A Bison Model 2350 A was used to generate the current and determine the apparent resistivity.

GENERAL DESCRIPTION OF FIELD SITES

The field resistivity observations were made at several sites in the discontinuous permafrost zone near Fairbanks, Alaska, and in the continuous permafrost zone near Prudhoe Bay, Alaska. The geology of the Fairbanks area and the region immediately to the north of it are characterized by a thick silt mantle overlying a Precambrian bedrock of schist (Péwé 1958). The silt is often perennially frozen with frequent occurrences of massive ice. The permafrost thickness is as great as 50 m and active layer depths are commonly between 30 and 100 cm. The sites near Prudhoe Bay have permafrost extending to depths greater than 600 m and surface materials are sand and gravel with a thin organic cap. The area is characterized by numerous pingos with lateral dimensions on the order of 30 m rising 5-10 m above the local ground surface. Much of the landscape is covered with shallow elongated lakes up to 2 km in length, with a few of them exceeding 2 m in depth. More detailed descriptions of the individual sites investigated are contained in the Results section.

RESULTS

Five studies of the effects of seasonal change in ground resistivity upon the MI and SI methods were

performed in Alaska at times near maximum thaw and maximum ground temperatures (September) and maximum frost penetration and minimum ground temperatures (April). At one site additional early summer measurements were made. Three of the studies were made at sites in the Fairbanks area. The remaining two studies were made at several locations in the Prudhoe Bay area. The sites contained a variety of ground ice types such as pore and lens ice, ice wedges and pingos.

Site 1 CRREL Permafrost Station, Fairbanks, Alaska

Site 1 is at a field facility maintained by the U.S. Army Cold Regions Research and Engineering Laboratory. It was established in 1946 for examining the long-term effects of surface cover on permafrost stability (Linell 1973a) and provides a range of ground conditions common to fine-grained sediments in the discontinuous permafrost zone. The site contains three one-acre plots, two of which have had their vegetative cover modified, as illustrated at the bottom of Figures 9 and 10.

The modifications significantly influenced permafrost distribution. Plot A retains its natural black spruce and moss (sphagnum) cover. From plot B only the trees and brush were removed. From plot C the surface vegetation was completely removed, including the entire organic layer; this resulted in deep thaw of the permafrost. The subsurface permafrost profile in Figure 9 is highly idealized and based on limited drilling performed in 1972. Our observations suggest that the subsurface situation in plot B, idealized in Figure 9 and 10, is the most complicated and that some permafrost may be returning. This may result from revegetation by the many small shrubs and trees that now cover this plot.

Figure 11 gives DC data from Arcone et al. (1978) taken in late June 1976 along the transects indicated in the bottom of the figure. These data are intended to verify quantitatively the MI and SI information obtained over the center of each plot. Figure 11 also shows layer models that were fitted to the DC data to interpret the subsurface layering. The models generally correspond to information obtained by drilling (Linell 1973a, 1973b). The plot A model suggests that ice-
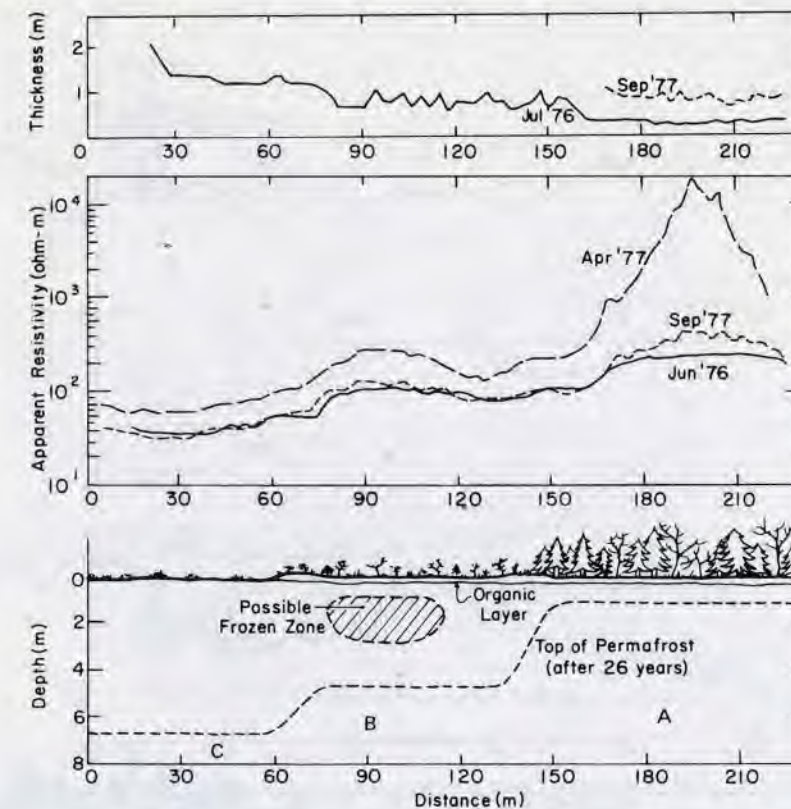

Figure 9. Magnetic induction apparent resistivity profiles across the CRREL permafrost test site in Fairbanks, Alaska (profile after Linell 1973). The top profile is active layer thickness.

rich permafrost may extend no more than 10 m deep; this is implied by the drilling south of this site at a lower elevation reported by Linell (1973b). The plot B model suggests that 1000-ohm-m material extends much deeper than the 5-m depth, but enough data points could not be obtained to effectively model the lower depths of this plot (the total spread at 20-m spacing already spanned the entire plot). The plot C model suggests that the thaw beneath the permafrost, or warm, less ice-rich permafrost, is about 300 ohm-m; but again, sufficient data points could not be obtained to absolutely confirm this.

Seasonal apparent resistivity profiles for the MI and SI (257 kHz) methods are given in Figures 9 and 10, respectively. Figure 9 presents the seasonal MI data along with seasonal information on depth of thaw of the active layer. No thawing of the active layer had yet occurred at the time of the early April observations. In late June 1976, thaw of the seasonally frozen ground had progressed to a depth of 30 to 40 cm in plot A, to 1 m in plot B, and to greater than 1 m in plot C with all seasonal frost completely disappearing at its southern

end. In September, depth of seasonal thaw was about 80 cm under plot A with seasonally frozen ground totally absent in plots B and C.

The influence of the seasonally frozen surface layer in April can be seen in Figure 9 on all plots, but especially on plot A where the active layer is frozen down to the permafrost. The early spring apparent resistivities increase over the late summer readings by as much as a factor of 40 at the center of plot A. These observations can be substantiated by theoretical computations. Because of the MI instruments' limited penetration depth, a simple 2-layer model of plot A, consisting of an 80-cm active layer over permafrost was assumed. Using active layer resistivities for the organic-rich silt of 100 ohm-m during late summer and 10,000 ohm-m during late winter, and permafrost (ice-rich silt) resistivities of 2000 ohm-m during late summer and 10,000 ohm-m during late winter, the ρ_a values are then 347 ohm-m for late summer and 12,600 ohm-m for late winter. These values are very close to the observations over the center of this plot made at a height of 1 m above ground (hip level).
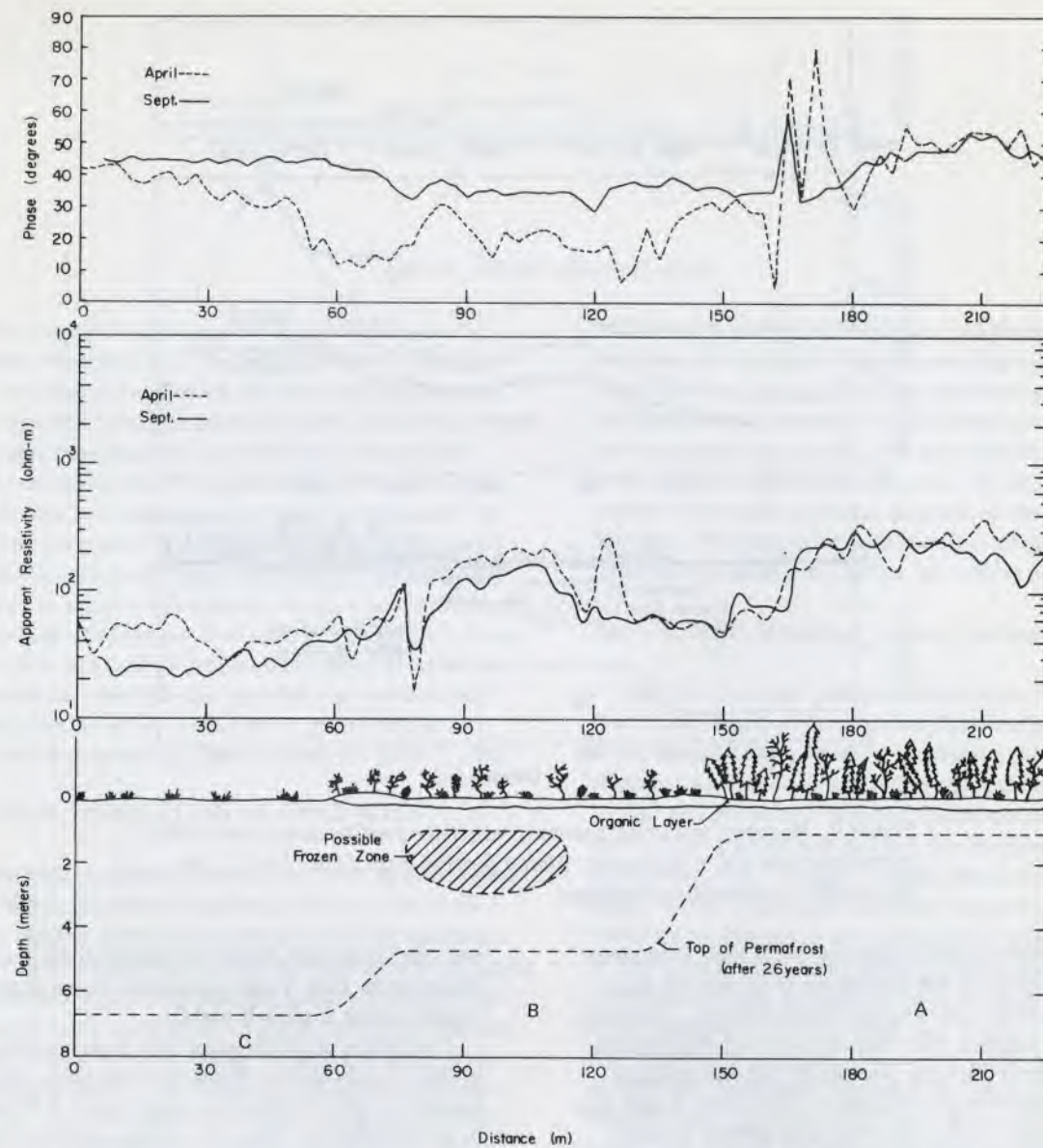
Figure 10. Surface impedance apparent resistivity and phase profiles at 257 kHz across the CRREL permafrost test site in Fairbanks, Alaska.
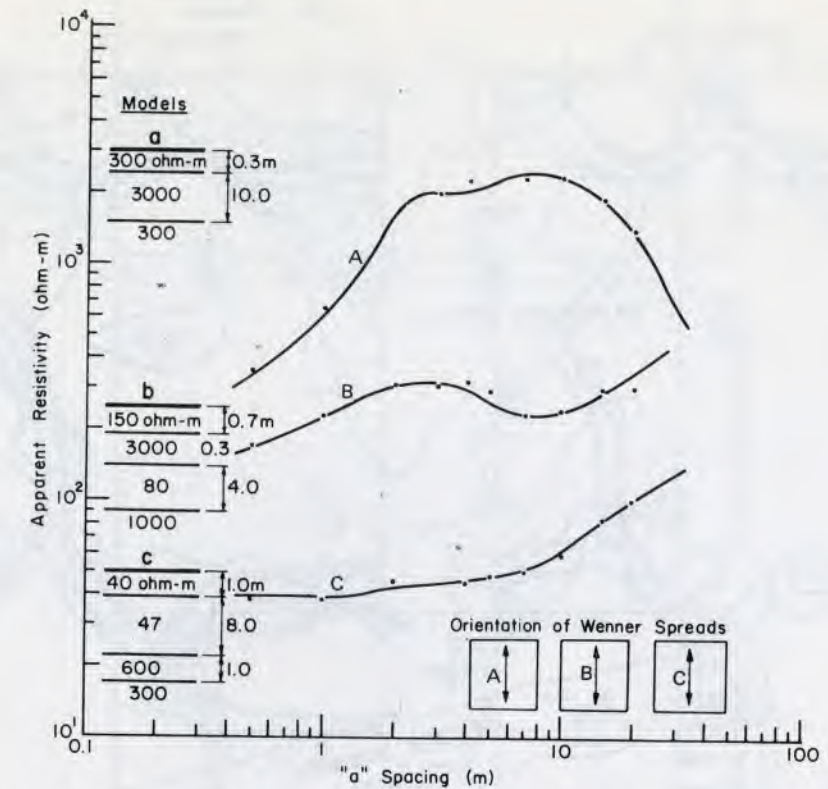

Figure 11. Galvanic sounding data (dots) obtained in late June over each plot of Figure 10 using the equispaced Wenner array configuration. The smooth curves matching the data were generated from the layered models shown at left.

Over plot C, ρ_a changes seasonally from between 30 and 40 ohm-m to between 70 and 80 ohm-m. A simple 2-layer model for a 1.3-m active layer over deep thawed silt gives a late summer ρ_a of 42 ohm-m when the active layer is 30 ohm-m and the deeper silt is at 40 ohm-m, and a late winter ρ_a of 80 ohm-m for a 10,000 ohm-m active layer over 50 ohm-m thaw. These values are similar to the data. The seasonal contrasts over plot B are similar to those over plot C.

The low-frequency SI data shown in Figure 10 show much less seasonal contrast than the MI data, probably because of the greater penetration of the radiowaves

into the material beneath the ice-rich permafrost, which may have a resistivity of no more than 300 ohm-m, as was suggested by the DC data for plot C. Using a summer model for the center of plot A, consisting of an 80-cm, 100-ohm-m active layer over a 10-m, 2000-ohm-m permafrost over 300-ohm-m thaw or warm permafrost with little ice, the theoretical SI value at 257 kHz is 558 ohm-m at 46.8°. The ρ_a is more than twice the ρ_a observed but the phase value is in good agreement. Using late winter values of 10,000 ohm for both the active layer and permafrost, the theoretical SI value is around 900 ohm-m at 65°, which is again greater than twice the observed ρ_a.

Improvements can be made in matching the observed and theoretical ρ_a values by decreasing the resistivity of the subpermafrost, but this would be at the expense of the good agreement between the theoretical and observed phase data. As can be seen from the SI data over plot C, in conductive material, all the instruments agreed; so we do not question the calibration of our instruments. This unusual amplitude behavior of the SI readings in high-resistivity ground will be seen at other sites, and some possible explanations are offered in the discussion of Site 4 and in Section VI. Over plot C, in late winter, the SI readings are around 40 to 60 ohm-m, and in late summer between 20 and 40 ohm-m. The skin depth at 40 ohm-m for a 257-kHz radiowave is about 6.3 m; this means that since this is less than the depth of the 30-40 ohm-m material, phases should be near 45° in late summer, which they are, and ρ_a should be similar to ρ_a, as measured by the MI method, which it is.

Site 2. Planned road cut for Steese Highway near Fox, Alaska

Site 2 is situated north of Fairbanks and was established by the University of Alaska Geophysical Institute

and Alaska Highway Department (Osterkamp and Jurick 1978). The site was positioned where a road cut was planned for the new Steese Highway. Preliminary Highway Department drilling indicated several areas of massive ice. The actual massive ice distribution was exposed during construction activity, as is shown at the bottom of Figure 12. This allowed direct correlations to be made between the resistivity readings and the actual materials present. In Figure 12, Qsu refers to Quaternary frozen silt and p€bc to the bedrock, Precambrian Birch Creek schist. The subsurface control was based on field sketches of the road cut made along the study line by the University of Alaska and Highway Department personnel.

The seasonal MI profiles of Figure 12 demonstrate the effect of the active layer and the warmer ground temperatures. In September, the resistivity contrasts over the massive ice are severely reduced from the large April contrasts. Over the sections containing no massive ice, the April data give resistivities as low as 400 ohm-m, and over the massive ice readings greater than 10,000 ohm-m. This represents a change by a factor of greater than 25 for frozen silt, caused primarily by ice content. The DC 3-m a spacing traverse
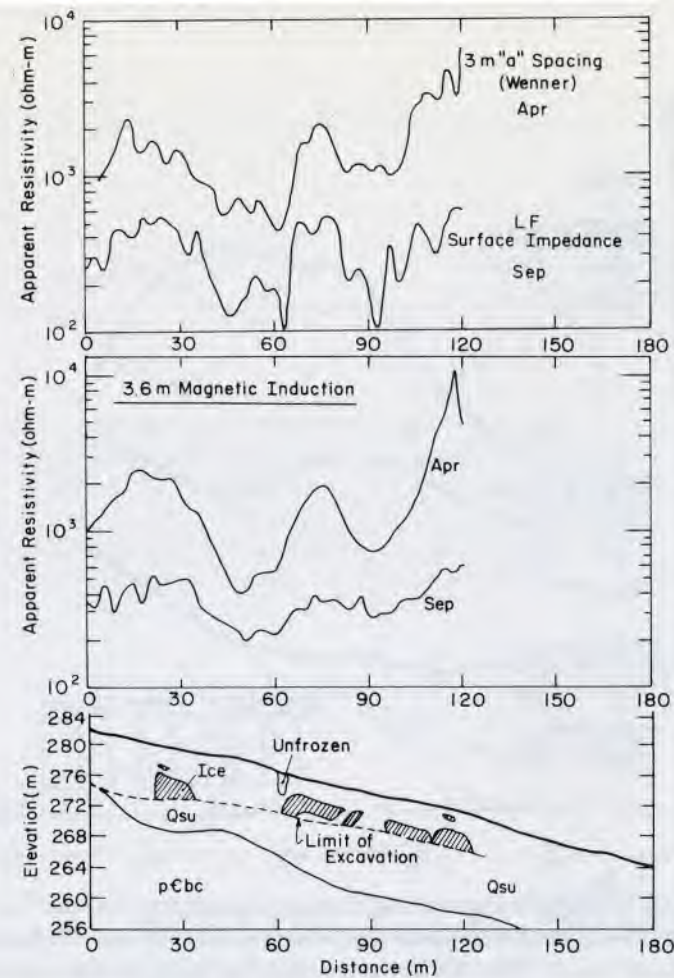
Figure 12. Apparent resistivity profiles using three different methods along a planned road cut for the Steese Highway near Fox, Alaska. Qsu, Quaternary frozen silt; pЄbc, bedrock, Precambrian Birch Creek schist.

gives almost identical results to the April MI data. The LF (257-kHz) ρ_a data are in the same range as the September MI data, but are more sensitive to the massive ice. The LF phases were commonly between 20° and 35°, reflecting the general increase of resistivity with depth.

Site 3. Relic floodplain near Fairbanks, Alaska

Site 3 is located in a relic floodplain of the Tanana River near Fairbanks, Alaska. Perennially frozen silt, sand and gravel may be capped by up to 6 m of organic silt containing numerous large masses of ground ice. The area is characterized by ice wedge polygons, which were mapped from the troughs overlying the polygonal wedge pattern. Probing of the active layer at 40 sites gave a range of thaw depth in September of 40 to 60 cm. The area was seasonally mapped using the SI method at 257 kHz. Data were taken on a 3-m grid spacing

with extra data points taken over the ice wedges.

The contoured low-frequency SI resistivity and phase data from September 1977 are shown superimposed upon the polygonal distribution of massive ice in Figure 13. Low phase anomalies and high resistivity anomalies occur over the massive ice. Over the troughs, values are typically greater than 7000 ohm-m and less than 10°, as compared with the mean values for the equispaced grid stations of 5011 ohm-m at 19°. Because resistivity increases near the surface of an ice wedge, one might expect phases there to exceed the mean. However, conventional plane wave interpretation techniques do not apply to such situations of lateral discontinuities in resistivity.

Figure 14 shows a very unexpected contrast between the resistivity data of September 1977 and April 1978 (phase data not shown). In both cases all the higher resistivity zones for both seasons are situated over the

a. Contours of Apparent Resistivity (ohm-m x 10³)
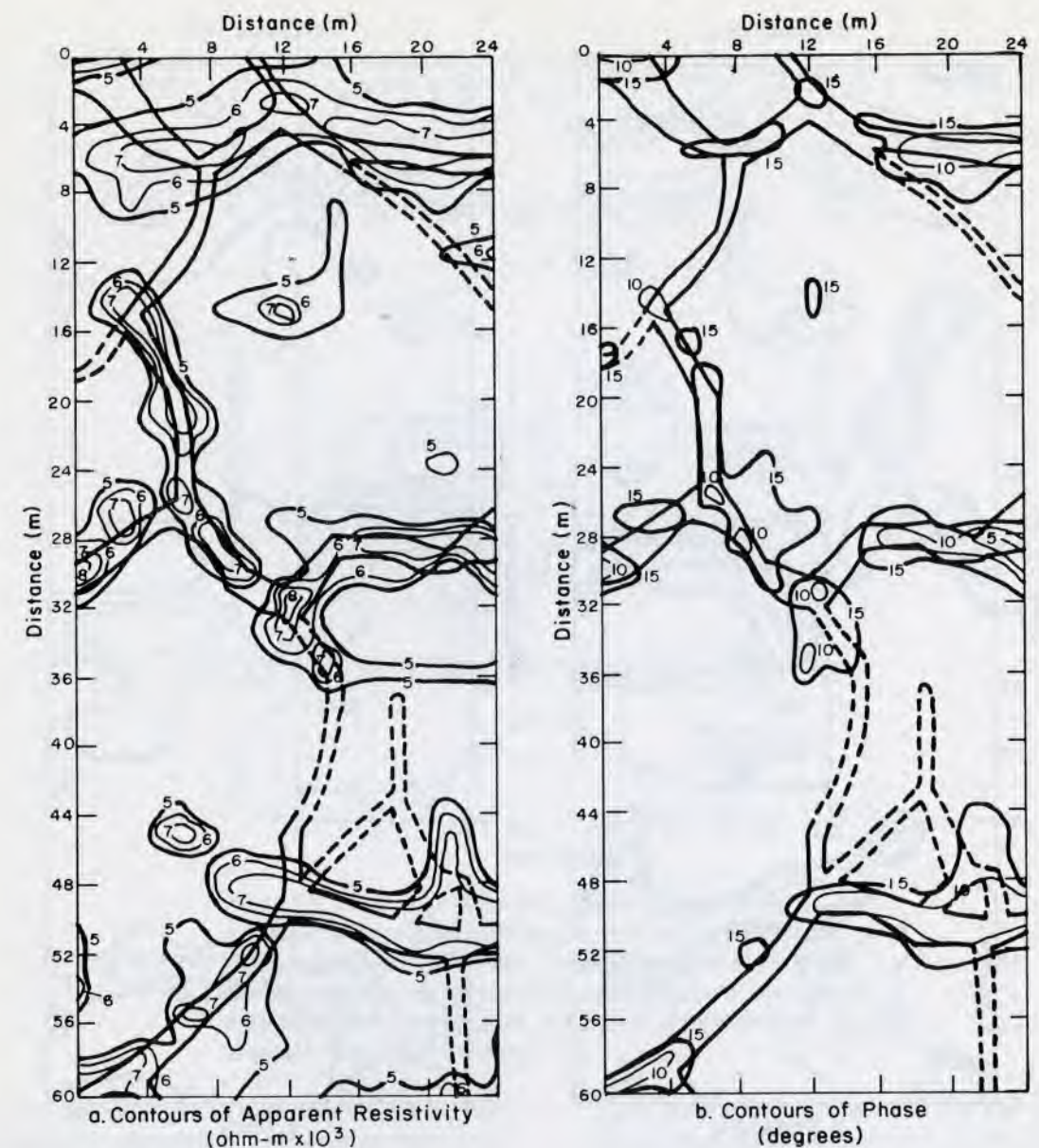
b. Contours of Phase (degrees)

Figure 13. September contours of apparent resistivity and phase at 257 kHz over a polygonal ground ice site near Fairbanks, Alaska. In this figure the polygonal boundaries are shown as dark lines and the questionable boundaries are broken lines.

ice wedges, but the general resistivity values are much lower for April than they are for September. The April mean resistivity value for just the equispaced grid points is 2870 ohm-m and the average phase is 60.5°, whereas the September means are 5011 ohm-m at 19°. Both these phase values are entirely plausible as the permafrost temperature in April increases with depth, whereas in September a thawed, conductive active layer exists. However, at the present time, we find the difference in apparent resistivity unexplained. In April, 63 separate determinations of resistivity, using the 15- and 30-m

VCP MI, gave average values of 2508 ohm-m and 426 ohm-m, respectively. At 3.66-m (HCP) spacing, the readings were greater than 10,000 ohm-m. Modelling based on these values indicates that our April LF readings were correct. Attempts to take MI measurements in September on two occasions were not successful because of instrument drift due to undetermined origin. We resurveyed this area the following September (1978), using the SI technique, and measured mean values of 5188 ohm-m at 23.6°, thus confirming the validity of the April-September contrast.
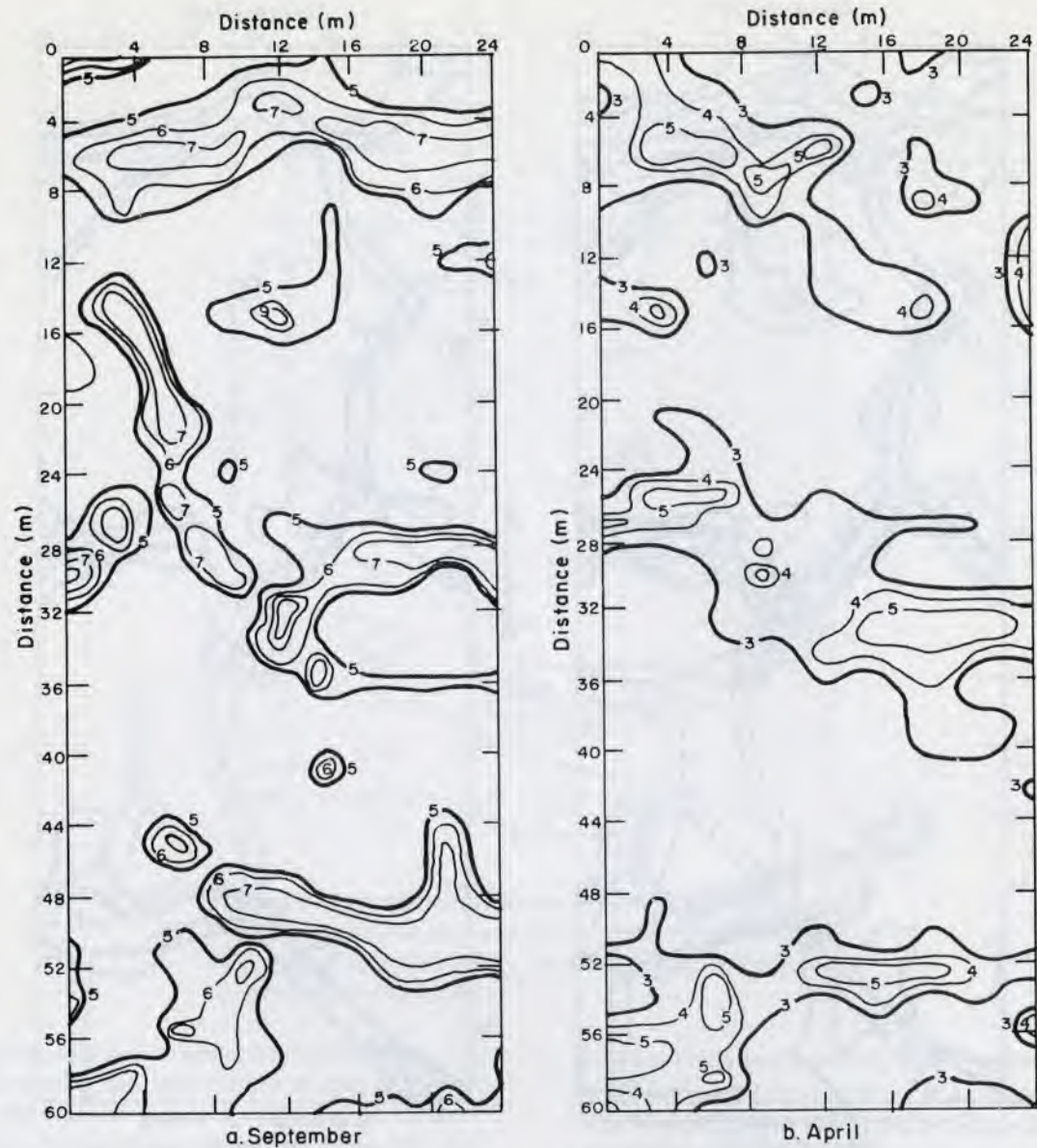
Distance (m)

a. September

Distance (m)

b. April

Figure 14. Seasonal contours of apparent resistivity at 257 kHz over the same site as in Figure 13.

It was also suspected that the several AM broadcast stations located within 2 miles of this site influenced the readings because their signal strengths were far in excess of the LF signal strength. This idea was discarded, however, after several measurements were taken later at a site in Claremont, New Hampshire, where both an AM broadcast station and an LF transmitter (1230 and 234 kHz, respectively) were aligned (their magnetic fields were parallel at the measurement site) and at similar distances. The measurements at the New Hampshire site revealed almost the same field strength ratios as those at Site 3. At the New Hampshire site, no difference was seen in the LF measurements between

times when the AM broadcast station was operating and when it was not.

Site 4. Pingos, Prudhoe Bay, Alaska

Two separate pingos were investigated in the Prudhoe Bay area of Alaska's North Slope, where permafrost is generally over 600 m thick. Pingos are growths of massive ice; in the Prudhoe Bay area they form mounds that rise to about 10 to 12 m above the surrounding surface. In this area, they are covered by a veneer of sand and gravel. One pingo was investigated in early April 1978, and the other in late September 1978.
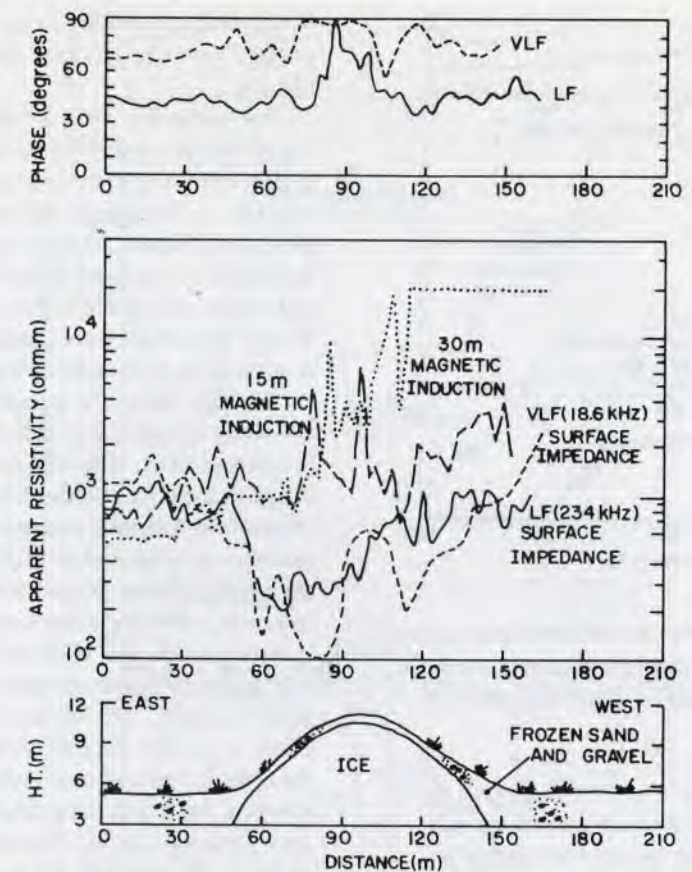

Figure 15. Magnetic induction ρ_a and surface impedance ρ_a and ϕ profiles taken in April 1978 across Prudhoe Mound pingo in Prudhoe Bay. At both LF and VLF, the direction of the transmitters is north to south so that the induced ground currents are generally directed north-south. At 3.66 m, the MI readings were all greater than 10,000 ohm-m.

The first pingo could not be reinvestigated in September because of the installation of a radio transmitter on its top by another research organization.

MI and SI measurements were made at several loop spacings and at two different frequencies, respectively. Readings were made every 3 m along single profiles crossing the pingo crests. Figure 15 shows the results for Prudhoe Mound, which was investigated in April when the air temperatures were between $-10°C$ and $-20°C$. At 3.66-m MI spacing in the HCP loop configuration, all the resistivities were greater than 10,000 ohm-m, indicating that, on the average, about the top 7 m of ground was this resistive. At the 15- and 30-m spacings, the vertical coplanar (VCP) loop configuration was used. On the east end of the traverse, the 15-m MI read between 600 and 1000 ohm-m and the 30-m MI read about 500 ohm-m. Both readings then rose sharply over the pingo and on the west end of the line remained higher than on the east end.

The April SI data were taken at 234 kHz and at 18.6 kHz. These ρ_a values are similar to the MI values at the east end and increase at the west end as do the MI readings. However, over the pingo, unexpectedly, at 18.6 kHz the resistivity obtained with the SI method dropped as low as 100 ohm-m and the 234-kHz values as low as 200 ohm-m, falsely representing the feature as a conductive anomaly. Correctly, though, both frequencies exhibited extremely high phases over the pingo, which usually indicates very sharp decreases in resistivity with depth.

Two possible explanations for the phase and amplitude behavior are as follows: 1) Both the LF and VLF transmitters are located to the south so that, under standard layering conditions, ground currents excited by the radiowave fields would be directed north-south. However, the massive ice is more extensive on the west end, as indicated by the MI readings. This localized ice
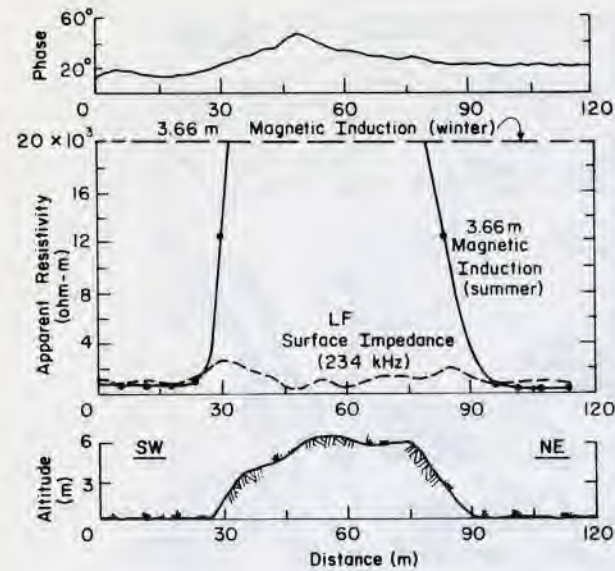
14

15

Figure 16. Surface impedance and magnetic induction apparent resistivity and SI phase profiles over a second pingo near Prudhoe Bay, Alaska. Data were taken in September 1978.

distribution could then force a serious directional distortion of the otherwise north-south ground current flow on the east side in order to avoid this highly resistive mass. Consequently, the ground tangential electric field in the north-south direction (but not necessarily the total electric field) would be greatly reduced on the east side of the ice mass. This would then make it appear as a conductive anomaly since our probes were oriented only in the north-south direction. Unfortunately, we did not determine the true direction of the ground tangential component of the electric field.

2) Topographic disturbances that are physically much less than a free space wavelength in size have been shown to cause a strong intensification and gradient with altitude of the vertical electrical field by Harrison et al. (1971) and by Arcone (1978). The effect is similar to that of any finitely conducting body placed within a static field. The effect is strongest at the body's surface, but attenuates rapidly at altitude when the body's dimensions are much smaller than the altitude in question. The divergence equation for the electric field, $\nabla \cdot \vec{E} = 0$, then requires that opposite changes also take place in the horizontal direction for the horizontal electric field so that the in-phase component of E_x decreases. This would then cause an increase in phase (determined by the arctangent of the ratio of the quadrature to in-phase components of the tangential electric field) as observed. The study by Arcone (1978) suggested that the SI is not affected at VLF over large mountains;

in that study, however, a very large mountainous area of high resistivity was examined, not a small, single feature.

The September 1978 MI and SI data are given in Figure 16 for another pingo located nearby, about 1 mile northeast of the Trans Alaska Pipeline Pump Station No. 1. This pingo rises about 7 m and had an active layer of about 30-40 cm of dry sand and gravel. It is situated to the northwest of the 234-kHz transmitter, and traverses with the 3.66-m MI unit and the 234-kHz SI unit were made from northeast to southwest, which is orthogonal to the transmitter direction.

The data imply that a much more symmetric ice distribution exists here, as is shown by the symmetry in the data profiles. The well-drained active layer had an insignificant effect on the 3.66-m MI data over the pingo because the instrument consistently indicated that resistivity was greater than 20,000 ohm-m. Off the pingo, the warm, summer ground temperatures and a conductive, wet, active layer decreased the ground resistivity to between 400 and 1000 ohm-m; this showed the contrast between the resistivities of the pingo and the adjacent material. The increase in SI phase and the decrease in ρ_a over the center of the pingo are similar to the effects observed over Prudhoe Mound during the previous April, and the probable causes of this behavior were explained above. The surface impedance phases of about 20° observed off the pingo reflect 1) the influence of the conductive active layer and 2) the decrease in temperature with depth through the effective depth of penetration of 234-kHz radiowaves. This effective depth of penetration is about 33 m for an apparent resistivity of 1000 ohm-m.

Site 5. Ice wedges, Prudhoe Bay, Alaska

This study was intended to compare the ability of the MI method in the HCP loop configuration to discern ice wedges with that of the same method in the VCP configuration. The investigation was conducted in the Prudhoe Bay area in September, which the above pingo studies had revealed was the time of optimum conditions for detecting massive ice. The exercise showed that the VCP configuration is most sensitive to inhomogeneities aligned with the intercoil axis, but that active layer properties in late summer can have a greater influence on observations than variations directly related to subsurface ice wedges.

Figure 17 shows the subsurface profile for the ice wedge site as inferred from the surface features of the polygonal ground. Over the ice wedges, thermal erosion has occurred and most of the troughs formed contained standing water which kept the active layer saturated. Therefore, the wedges appear as low-resistivity anomalies
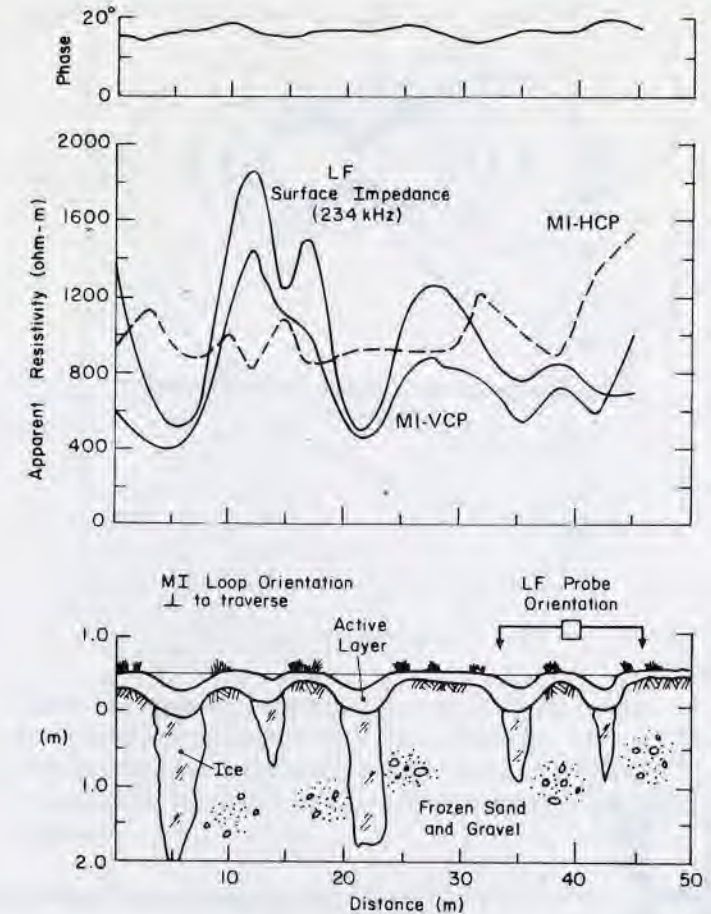

Figure 17. Magnetic induction and surface impedance apparent resistivity and surface impedance phase profiles over an ice wedge site near Prudhoe Bay, Alaska. Data were taken in September 1978.

for the VCP orientation, which has much greater sensitivity than the HCP orientation to a thin conducting layer at the surface. (Compare Fig. A3 and A4 (App A) for an interloop spacing $s = 3.66$ m.) In both cases, the instrument (interloop) axis was aligned parallel with the wedges.

The greater VCP sensitivity to the wedge-trough area also results from the constriction of the primary magnetic field of a loop antenna toward the plane that contains the loop, as shown in Figure 18. When the plane of the loop is horizontal (HCP) (Fig. 18a), the primary magnetic field is constricted toward the horizontal plane; and when the plane is vertical (VCP) (Fig. 18b), the field is constricted toward the vertical plane. Therefore, in the VCP orientation, the instrument is more sensitive to the ground directly underneath the interloop axis, which is aligned with the wedge-trough direction.

Figure 17 also presents SI (234-kHz) data. Here, the tangential electric field direction was orthogonal to the wedge orientation. The variations in ρ_a practically parallel those of the VCP MI unit, and the ρ_a values are less on the average than those of either the HCP or VCP MI configurations. The phase data reflect the sharp increase of resistivity with depth because the phase angles are between 14° and 20°. The phase is stable in comparison with ρ_a.

The SI observations allow resistivity values for the frozen and thawed ground to be estimated using a simple two-layer model of a conductive active layer over resistive permafrost, as presented in Figure 19. This figure shows that an active layer of 50-cm thickness decreases the apparent resistivity at 234 kHz of the permafrost from 5,000 ohm-m to 1400 ohm-m, while between 20- and 60-cm depth the phase varies only between 26° and 17°. These data are close to the
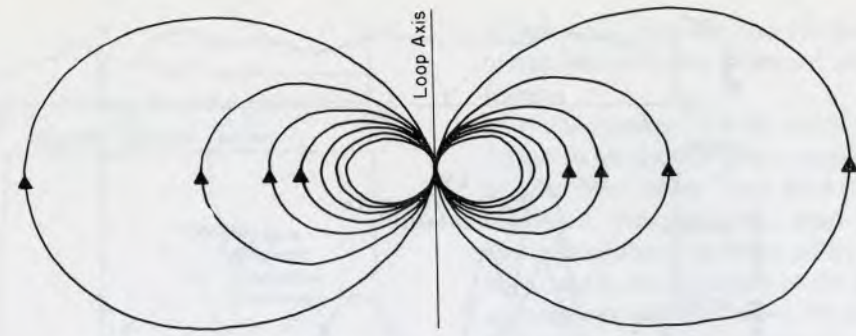
a. The horizontal coplanar (HCP) orientation.
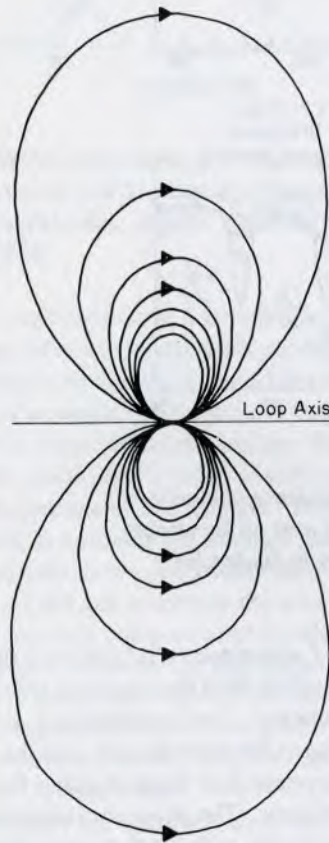
b. The vertical coplanar (VCP) configuration.

Figure 18. Cross section of the primary magnetic field produced by the transmitter antenna loop as seen from the receiver loop. The three-dimensional field is obtained by rotating the field pattern about the loop axis. In the VCP orientation, the field is more confined to the vertical plane that contains the interloop axis, and, therefore, to the ground directly beneath the interloop axis.
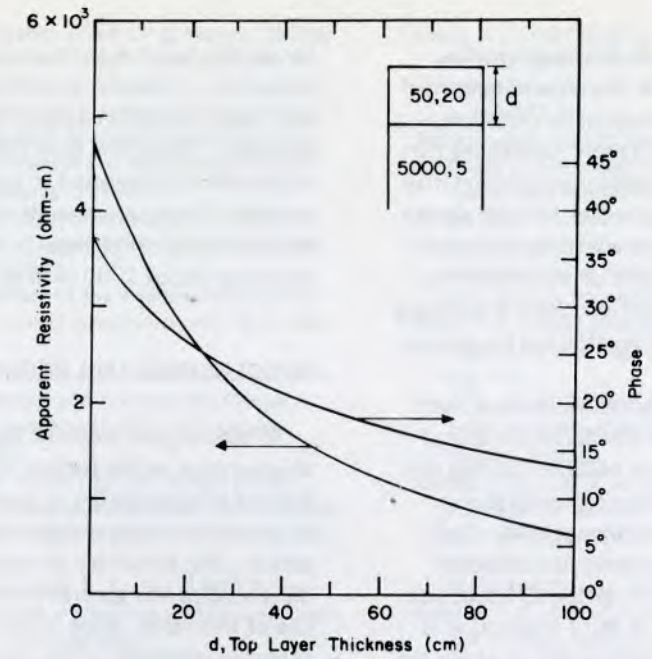

Figure 19. Apparent resistivity and phase at 234 kHz above a two-layer ground model of thaw over permafrost. The first number in the layers gives the model value of resistivity in ohm-m and the second number is an approximate dielectric constant.

observations made over the sections without standing water (Fig. 17) and suggest that the ice features do not differ significantly in resistivity from the frozen sand and gravel. The resistivity variations seen in all methods are primarily responses to changes in the active layer and in the standing water.

COMPARISONS BETWEEN THE SURFACE IMPEDANCE AND MAGNETIC INDUCTION METHODS

The standard data interpretation procedure for both MI and SI methods is based on the earth model of vertically stratified homogeneous layers. In reality, shallow layering, when it occurs, is usually local, and what the lateral extent of the layering must be in order to use the standard interpretation procedure is not known. However, estimates of this extent might be as described in the following:

SI method. Subsurface inhomogeneities produce scattered electromagnetic fields. Since any electromagnetic field can be mathematically resolved into an infinity of plane waves all propagating at various angles from the scatterer, the effect of a local disturbance is ultimately limited by the skin depth phenomenon for propagation in lossy (i.e., conductive) material. Therefore, we may expect that departures from homogeneity or homogeneous layering do not have an appreciable effect if the inhomogeneity is at least a skin depth away in the material considered. In very resistive ground, for example, ground of 1000 ohm-m resistivity, the skin depth at 250 kHz is 32 m; therefore, inhomogeneities within this distance from the point of measurement might well influence the data.

MI method. In this method, instruments are designed so that the ground penetration of the primary field is determined only by the interloop spacing and by the loop orientation. Therefore, the effective depth of penetration is always fixed (e.g., about 7 m for the 3.66-m system in the MI HCP configuration), so that localization of the measurement is known. The MI system is therefore superior to the SI system in distinguishing local variations. These arguments probably explain why the MI method was less erratic than the SI method when used to follow the subsurface geology at Sites 1 and 2 in this study.

The data intepretation for the SI method also depends on the plane wave assumption, which in turn demands that only vertically stratified homogeneous layers exist. A plane wave is one for which the phase and amplitude of the electric and magnetic field components are

constant along infinite planes. In the pingo studies, however, there was evidence that the ground tangential electric field may have been directionally distorted across the resistive ice mass, thus falsely identifying part of it as a conductive area. The same phenomenon may have been taking place around, over, or beneath the ice wedges at Sites 3 and 5. Also, data were undoubtedly influenced by the fixed orientation of the transmitter relative to the ice masses. In addition, there is evidence that the ground SI method may be affected by surface topography.

In contrast to the SI method, the MI method has the versatility of making measurements in any lateral orientation. This is advantageous because rotating the interloop axis in a horizontal plane can average out inhomogeneities beneath the instrument used. Also, measurements can be made in at least two different loop orientations (HCP and VCP), giving different penetrations for one loop spacing. A third orientation is possible for the Geonics EM34 instrument in which the planes of the loops are vertical but face each other in a coaxial arrangement. Topography, also, is not a problem with this instrument as long as the dimensions of the relief are much larger than the interloop spacing.

The main advantages of the SI method are: 1) Under reasonably ideal conditions, measurements at VLF in highly resistive ground are indicative of far greater depths than present commercial MI systems can obtain. For example, at 2,500 ohm-m, the skin depth at 20 kHz is about 180 m, which exceeds the maximum depth of permafrost in some northern regions. 2) At any particular frequency, two pieces of data, namely amplitude and phase, are available. Theoretically, these data are also available with the MI method, but since the interpretation is far more difficult, only the quadrature phase component of the secondary coupling is used. 3) Theoretically, measurements may be made throughout the entire radio frequency range. Practically, however, this is not feasible because the earth's dielectric (polarization) properties are almost certainly influential above 1 MHz, and there are no transmitters operating below 15 kHz. This is remedied somewhat by the use of natural atmospheric emissions between 0 and 10 kHz in the magnetotelluric method, but then penetration becomes too deep to help interpret surface detail. A practical limitation in Alaska is the lack of suitable VLF and LF signal strength in many areas.

Both the SI and MI methods run into theoretical and practical difficulties when ground resistivity is very high, i.e., above about 10,000 ohm-m. In the LF range, dielectric properties begin to influence the readings for the SI method. For the MI method, operating frequencies

are usually too low to be concerned with dielectric properties. However, insufficient coupling of the secondary fields makes it extremely difficult to obtain much accuracy. Therefore, only the SI method is viable when resistivities are expected to generally exceed 10,000 ohm-m. Conversely, the MI technique is much more sensitive to minor changes in resistivity when resistivities are below about 1000 ohm-m.

CONCLUSIONS AND RECOMMENDATIONS

In general, the magnetic induction technique is probably superior to the surface impedance technique for shallow ground studies of permafrost distribution and of massive ice occurrences performed during the optimum season. The resistivity of massive ice encountered in these studies was generally 10,000 ohm-m or greater. Use of this value, along with careful estimates of the expected resistivity of the surrounding earth material, is required to estimate the ability of this technique to find large ice masses. It is also important to utilize the several antenna loop orientations available and to rotate the intercoil axis during surveys. Generally, the use of several techniques is recommended because it can increase the period for making measurements, provide more information, and permit cross checks on results obtained using any one method.

Certain conclusions may also be made as to the optimum time of year to conduct electromagnetic surveys in permafrost regions. Intuitively, late winter conditions seem ideal, because this is when ground resistivity is highest and there is no active layer thaw to rapidly attenuate radiowaves or mask out the effects of deeper, induced magnetic fields. This was certainly the case demonstrated in Figure 12, at Site 2, where the ice masses at depth in the frozen silt were revealed most clearly by the 3.66-m MI method in early April. However, in the pingo studies at Site 5, greater resistivity contrasts between the frozen sand and gravel and the massive ice occurred in September when the ground had warmed considerably. The early spring pingo measurements revealed that the frozen ground could become just as resistive as the massive ice. Therefore, in planning the time of year for a survey, it is recommended that geology, as well as season, be considered.

LITERATURE CITED

Annan, G.P. and J.L. Davis (1976) Impulse radar sounding in permafrost. *Radio Science*, vol. 11, no. 4, p. 383-394.

Arcone, S.A. (1978) Investigation of a VLF airborne resistivity survey conducted in northern Maine. *Geophysics*, vol. 43, no. 7, p. 1399-1417.

Arcone, S.A., P.V. Sellmann and A.J. Delaney (1978) Shallow electromagnetic investigations of permafrost. *Proceedings of Third International Conference on Permafrost*, National Research Council of Canada, p. 501-507.

Bhattacharyya, B.K. (1955) Electromagnetic induction in a two-layer earth. *Journal of Geophysical Research*, vol. 60, no. 3, September, p. 279-288.

Cagniard, L. (1953) Basic theory of the magneto-telluric method of geophysical prospecting. *Geophysics*, vol. 18, p. 605-635.

Crory, F. (1960) Discussion of pile construction in permafrost. *Journal of the Soil Mechanics and Foundation Division, Proceedings of the American Society of Civil Engineers*, vol. 86, no. SM4, p. 87-94.

Davis, J.L., W.J. Scott, R.M. Morey and A.P. Annan (1976) Impulse radar experiments on permafrost near Tuktoyaktuk, Northwest Territories. *Canadian Journal of Earth Sciences*, vol. 13, p. 1584-1590.

Delaney, A.J., P.V. Sellmann and S.A. Arcone (1978) A magnetic induction technique for shallow subsurface exploration. CRREL Technical Note. (Unpublished)

Harrison, R.P., J.L. Hecksher, and E.A. Lewis (1971) Helicopter observations of very low frequency waves over certain mountains and shorelines. *Journal of Atmospheric and Terrestrial Physics*, vol. 33, p. 101-110.

Hoekstra, P. (1978) Electromagnetic methods for mapping shallow permafrost. *Geophysics*, vol. 43, no. 4, p. 782-787.

Hoekstra, P. and D. McNeill (1973) Electromagnetic probing of permafrost. *Proceedings of North American Contribution to Second International Conference on Permafrost*, NRC-NAS, p. 479-498.

Hoekstra, P., P.V. Sellmann, and A. Delaney (1975) Ground and airborne resistivity surveys of permafrost near Fairbanks, Alaska. *Geophysics*, vol. 40, no. 4, p. 641-656.

Hopkins, D.M., et al. (1955) Permafrost and groundwater in Alaska. U.S. Geological Survey, Professional Paper 264-F.

Hughes, W.J. and J.R. Wait (1975) Effective wavetilt and surface impedance over a laterally inhomogeneous two-layer Earth. *Radio Science*, vol. 10, no. 11, p. 1001-1008.

Jackson, J.D. (1962) *Classical electrodynamics*. New York: John Wiley and Sons, Inc.

Jordan, E.C. and K.G. Balmain (1968) Electromagnetic waves and radiating systems, 2nd Edition. Englewood Cliffs, New Jersey: Prentice-Hall, Inc.

Keller, G.V. and F.C. Frischknecht (1966) *Electrical methods in geophysical prospecting*. New York: Pergamon Press.

Kovacs, A. and R.M. Morey (1979) Remote detection of massive ice in permafrost along the Alyeska pipeline and the pump station feeder gas pipeline. *Proceedings of the ASCE Pipeline Specialty Conference*, American Society of Civil Engineers, New Orleans, Louisiana, January 1979.

Lachenbruch, A.H. (1962) Mechanics of thermal contraction cracks and ice wedge polygons in permafrost. Geological Society of America Special Paper no. 70.

Linell, K.A. (1973a) Long-term effects of vegetation cover on permafrost stability in an area of discontinuous permafrost. *Proceedings of North American Contribution to Second International Conference on Permafrost*, NRC-NAS, p. 688-693.

Linell, K.A. (1973b) Risk of uncontrolled flow from wells through permafrost. *Proceedings of North American Contribution to Second International Conference on Permafrost*, p. 462-472.

MacKay, D.K. (1969) Electrical resistivity measurements in frozen ground, Mackenzie Delta Area, Northwest Territories. Association Internationale d'Hydrologie Scientifique.

Osterkamp, T.E. and R. Jurick (1978) Geophysical investigations at the Engineer Creek road cut, Fairbanks, Alaska. Paper presented at the Permafrost Geophysics Conference, Calgary, Canada, November 1978.

Péwé, T.L. (1958) Geology of the Fairbanks (D-2) Quadrangle, Alaska, U.S. Geological Survey Geological Quadrangle Map CQ-110.

Péwé, T.L. (1974) Geomorphic processes in polar deserts, from *Polar Deserts and Modern Man*, University of Arizona Press, Tucson, Arizona.

Rennie, J.A., D.E. Reid and J.D. Henderson (1978) Permafrost extent in the southern fringe of the discontinuous permafrost zone, Fort Simpson, N.W.T. *Proceedings of Third International Conference on Permafrost*, National Research Council of Canada, p. 439-444.

Rossiter, J.R., G.A. LaTorraca, A.P. Annan, D.W. Strangway and G. Simmons (1973) Radio interferometry depth sounding: Part II-Experimental results. *Geophysics*, vol. 38, no. 3, p. 581-599.

Rossiter, J.R., et al. (1978) Electromagnetic sounding of permafrost, N.W.T., Canada, in summer and winter. *Proceedings of Third International Conference on Permafrost*, National Research Council of Canada, p. 568-572.

Sinha, A.K. (1976) Determination of ground constants of permafrost terrains by an electromagnetic method. *Canadian Journal of Earth Sciences*, vol. 13, p. 429.

Stratton, J.A. (1941) *Electromagnetic theory*. New York: McGraw-Hill Book Company, Inc.

Telford, W.M., L.P. Geldart, R.E. Sheriff and D.A. Keys (1976) *Applied geophysics*. Cambridge University Press, New York.

Wait, J.R. (1970) *Electromagnetic waves in stratified media*. New York: Pergamon Press, 2nd Ed.

Wenner, F. (1915) A method of measuring earth resistivity. U.S. Bureau of Standards Bulletin 12.

Wong, J., J.R. Rossiter, G.R. Olhoeft, and D.W. Strangway (1977) Permafrost: Electrical properties of the active layer measured in situ. *Canadian Journal of Earth Sciences*, vol. 14, no. 4, p. 582-586.

DISCUSSION OF THE DEPTH OF SENSITIVITY OF THE MAGNETIC INDUCTION METHOD USING TWO- AND THREE-LAYER APPARENT RESISTIVITY CURVES

In this section we will attempt to give the reader some familiarity with the depth of sensitivity of the magnetic induction method. The mathematical development of the field expressions (e.g., Bhattacharyya 1955) is far more complicated than that for the plane wave surface impedance method and no simple parameter such as the skin depth (eq 7) applies. Instead, we will present some curves illustrating the variation of apparent resistivity with layer depth for a two- and three-layer earth and draw some conclusions from them for both the horizontal coplanar (HCP) and the vertical coplanar (VCP) loop orientations. These curves were generated from formulas supplied by Geonics Ltd. of Mississauga, Ontario.

Figures A1 and A2 illustrate the theoretical variation of apparent resistivity in the HCP and VCP modes respectively as a function of layer depth for a two-layer ground model where the resistivity ratio k of the layers is variable. The depth of the layer t is normalized by the loop separation s, and the apparent resistivity ρ_a is normalized by the first-layer resistivity ρ_1. Both figures show
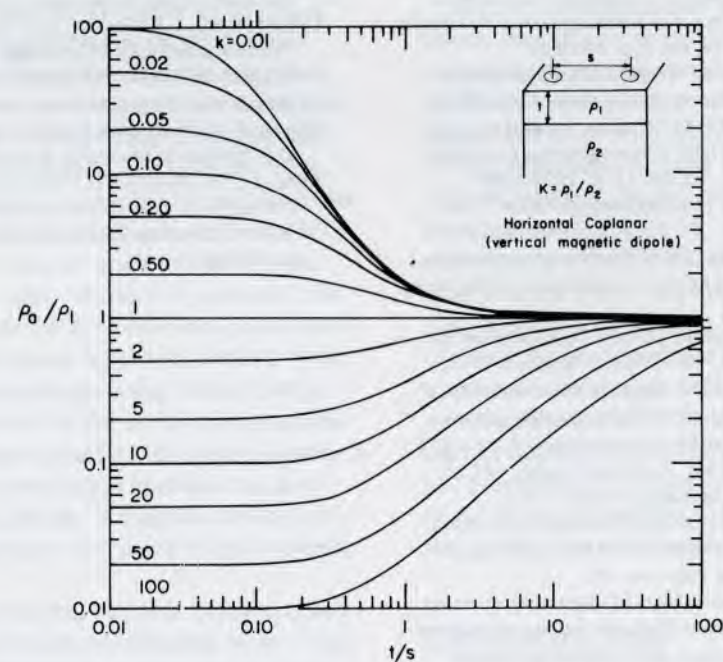
that in the case of a more conductive first layer, very little change in ρ_a occurs for both orientations when t exceeds about 2 s. However, at small values of t/s, the VCP orientation shows much greater sensitivity to the depth of a more conductive top layer than does the HCP orientation. With a less conductive top layer, the second layer affects ρ_a at much greater depths, especially for values of $k = \rho_1/\rho_2$ of 10 or more. Both orientations are only sensitive to large values of t/s when the first layer is much more resistive than the second.

Figures A3 and A4 illustrate the theoretical ability of the two orientations to detect a conductive thin layer at depth using the interloop distances available with the Geonics EM31 and EM34 instruments. The thin layer is 20 cm thick at 10 ohm-m and varies in depth within 1000 ohm-m ground. The HCP curves of Figure A3 show the most interesting behavior. When the interloop spacing $s = 3.66$ m, the thin layer gives maximum effect when its depth d is slightly greater than 1 m and lowers the apparent resistivity of the otherwise homogeneous ground by about 80%. By 10-m depth, the apparent resistivity has climbed to within 75% of 1000 ohm-m. When $s = 15$ and 30 m, the value $\rho_a = 750$ ohm-m occurs at depths of 19 and 24 m, respectively.

The VCP curves of Figure A4 behave differently at shallow depths, but behave similarly to the HCP mode
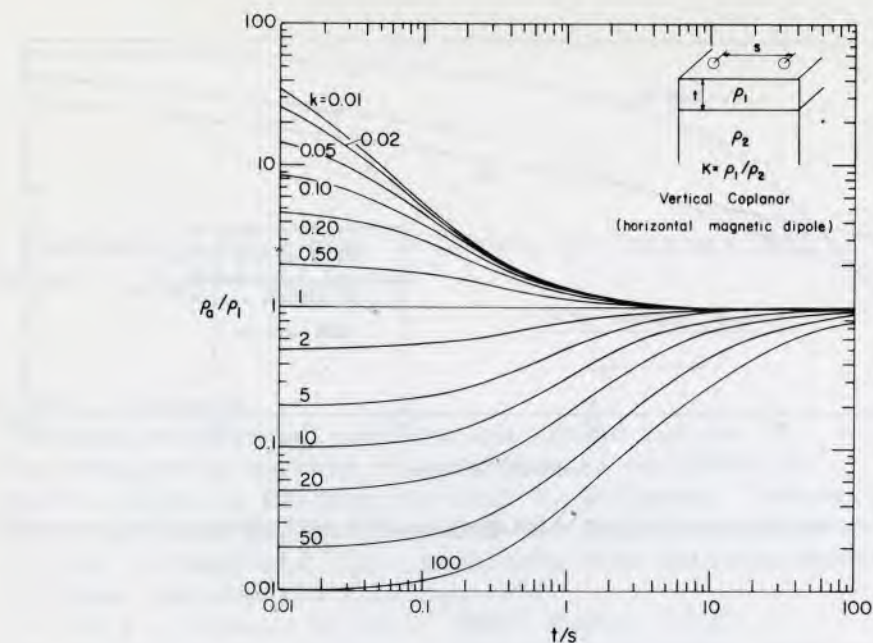

Figure A2. Normalized apparent resistivity as a function of normalized first-layer depth for the vertical coplanar orientation.
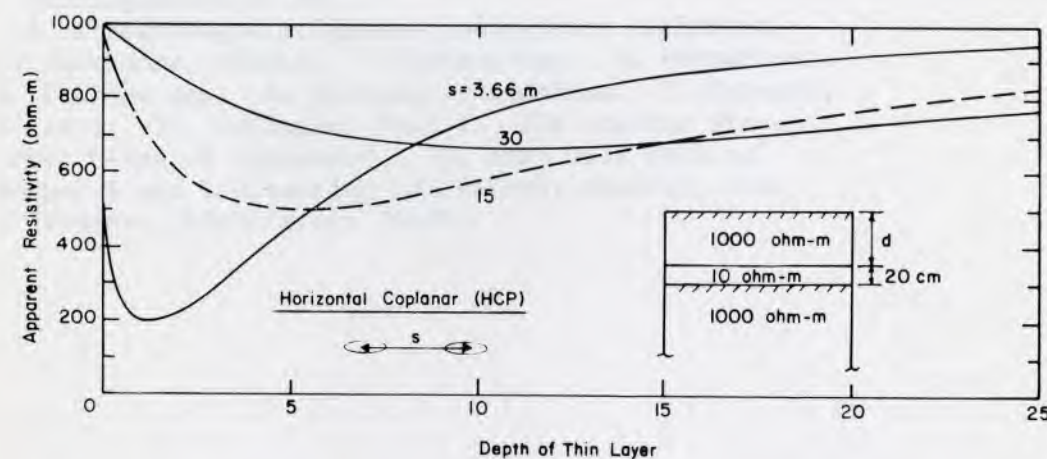

Figure A3. Apparent resistivity as a function of depth to a thin conductive layer for the horizontal coplanar loop orientation.

at greater depths. The VCP sensitivity to the thin layer when this layer is at or near the surface is much greater than that of the HCP mode for all values of s. For example, at 0.5-m depth, the HCP reading is 250 ohm-m at $s = 3.66$ m, but the VCP reading is 115 ohm-m. Between 1 and 5-m depth, the VCP response is nearly linear with depth at $s = 3.66$ m, as are the $s = 15$ and 30 m curves out to about 10 m and 17 m, respectively.

The above figures allow some generalizations to be made concerning the theoretical depths of sensitivity

of the Geonics EM31 and EM34 instruments. The EM31 ($s = 3.66$ m) is most effective over depths of about 7 m or less in both modes with the VCP mode offering the greatest sensitivity to a shallow conductive layer within about two meters. The EM34 gives the greatest depth sensitivity when it is in the HCP mode and when $s = 30$ m. Generally, the EM34 is effective to about a 17-m depth at $s = 15$ m and to about 25-m depth at $s = 30$ m.
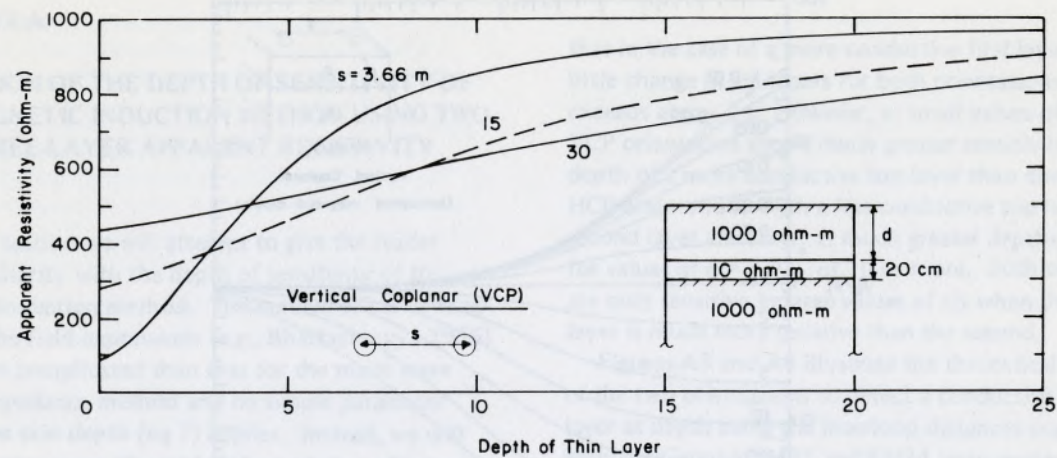

Figure A1. Normalized apparent resistivity as a function of normalized first-layer depth for the horizontal coplanar orientation.

Figure A4. *Apparent resistivity as a function of the depth to a thin conductive layer for the vertical coplanar loop orientation.*

A facsimile catalog card in Library of Congress MARC format is reproduced below.